Supplement of Earth Surf. Dynam., 9, 995–1011, 2021
https://doi.org/10.5194/esurf-9-995-2021-supplement

Earth Surface Dynamics
Open Access
EGU

Supplement of

Controls on the grain size distribution of landslides in Taiwan: the influence of drop height, scar depth and bedrock strength

Odin Marc et al.

Correspondence to: Odin Marc (odin.marc@get.omp.eu)

Supplement

Abstract.

This file contains 10 supplementary figures.

Supplementary Figure 1 shows the comparison between landslide volume estimated on the field and estimated from scaling relationships.

Supplementary Figures 2 and 3 are pictures showing part of LS-2 and LS-5.

Supplementary Figures 4 and 5 are showing the agreement between the empirical CDF of the landslide GSD and Weibull and Lognormal distributions.

Supplementary Figure 6 is similar to Figure 3B and shows the difference in GSD between the toe and apex of the deposit of LS-8 and LS-10.

Supplementary Figure 7 is showing the correlation between the D_{50} and the other percentiles of the 20 GSD distributions.

Supplementary Figure 8 is showing that there is no clear correlation between the Interquartile ratio (spread of the distribution) and the other percentiles.

Supplementary Figure 9 shows the effect of using different method to compute scar thickness when comparing our data to the fragmentation scaling proposed by Locat et al., 2006.

Supplementary Figure 10 shows the scar gradient and transport length for the surveyed landslides with and without signs of grain size segregation.

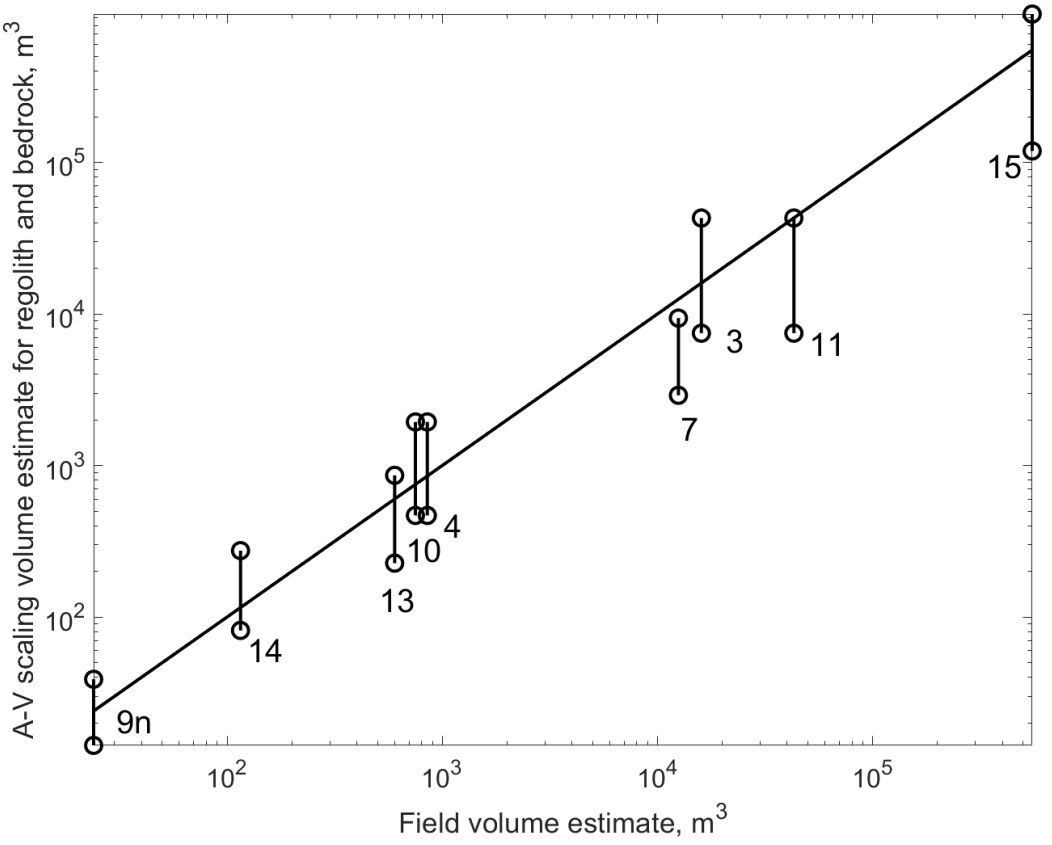

Figure S1. Volume estimated from bedrock or regolith scaling relationships (upper and lower circle, respectively) against the one estimated in the field assuming a half or quarter cone geometry.

Figure S2. Drone picture above a section of the transport channel of LS-2. Note the carapace of very coarse boulders ($> 1\ m$, see black and white target square of 1x1m for scale indicated by red arrows) on the left part of the channel. On the right part the carapace is missing or eroded and finer and more variable grain sizes are visible.

Figure S3. Picture of LS-5, with the approximative areas where we sampled the fan and transport channel of the deposit. Note the abundance of coarse blocks in the channel going up until the scar, which contrasts with the fan part to the left where coarse grains are inside a matrix of fine grains. Thus we consider likely that the deposit was reactivated due to river incision of its toe, and that the outcropping fan is more representative of the inner part of the deposit.

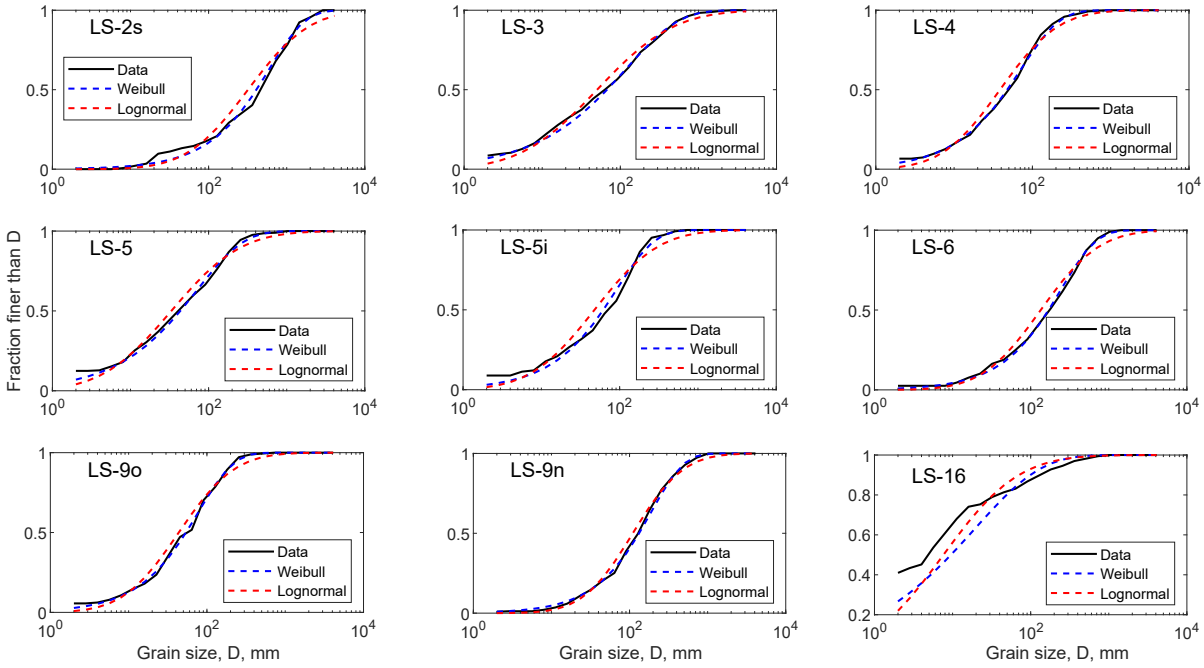

Figure S4. ECDF of the landslide grain size distribution and best fit Weibull and Lognormal distributions. These panels contains the landslide GSD with better fit by a Weibull distribution, and LS-16 which is poorly fit by both Weibull and Lognormal distributions.

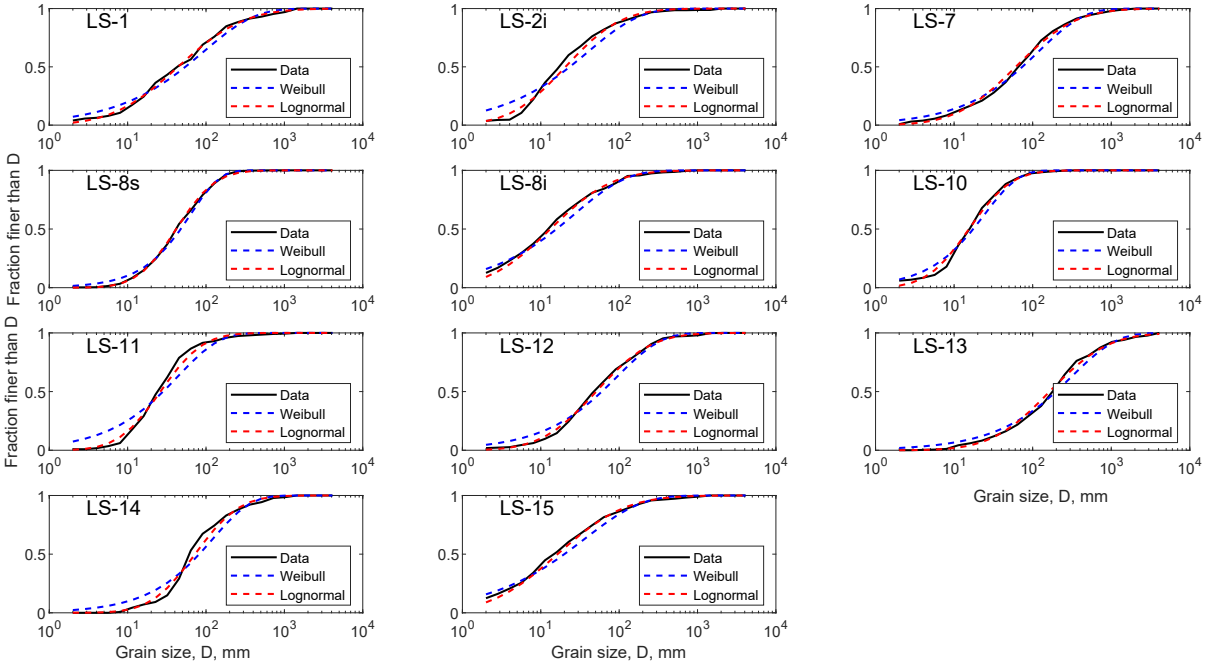

Figure S5. ECDF of the landslide grain size distribution and best fit Weibull and Lognormal distributions. These panels contains the landslide GSD with better fit by a Lognormal distribution.

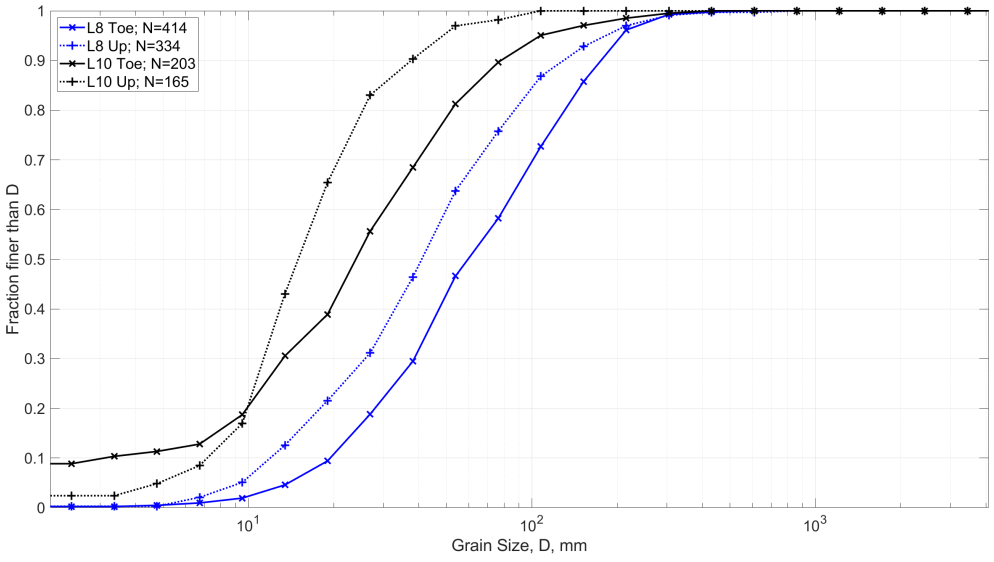

Figure S6. Downslope segregation in LS-8 and LS-10, similar to what is shown in Fig. 3B.

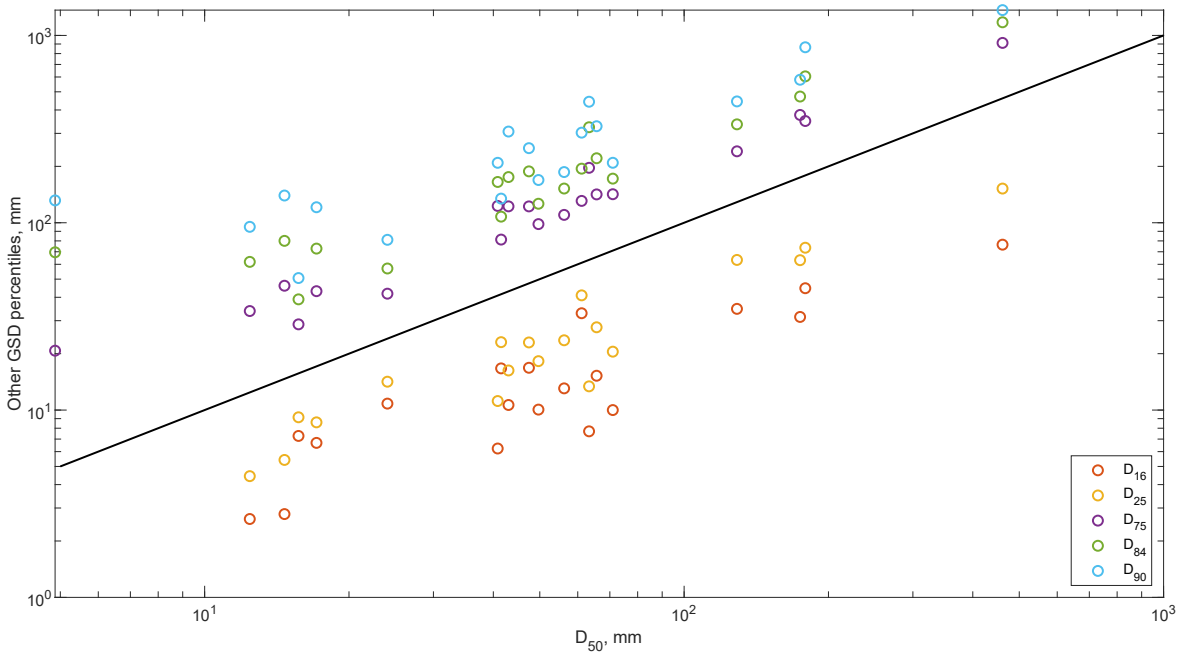

Figure S7. D_{50} against the other percentiles of the 20 landslide GSDs. Note that we could not determine the 16th and 25th percentiles of LS-16 as about 40% of the deposit was finer than our minimum grain size bin.

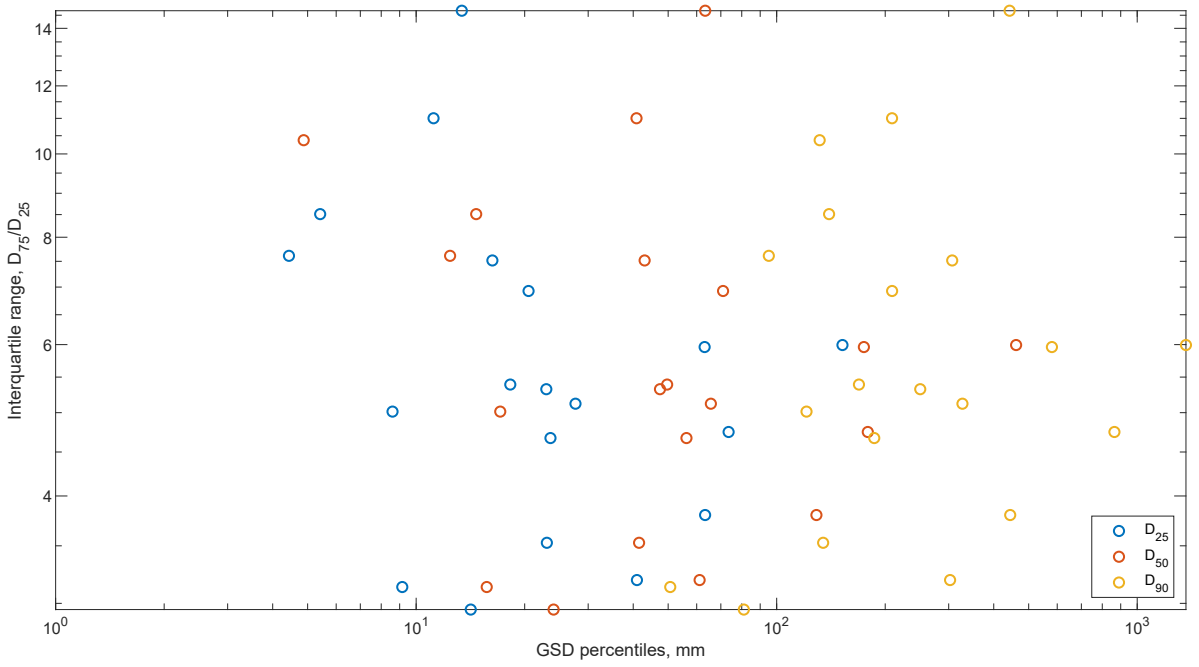

Figure S8. Interquartile ratio against the D_{25}, D_{50} and D_{90} of the 20 GSDs.

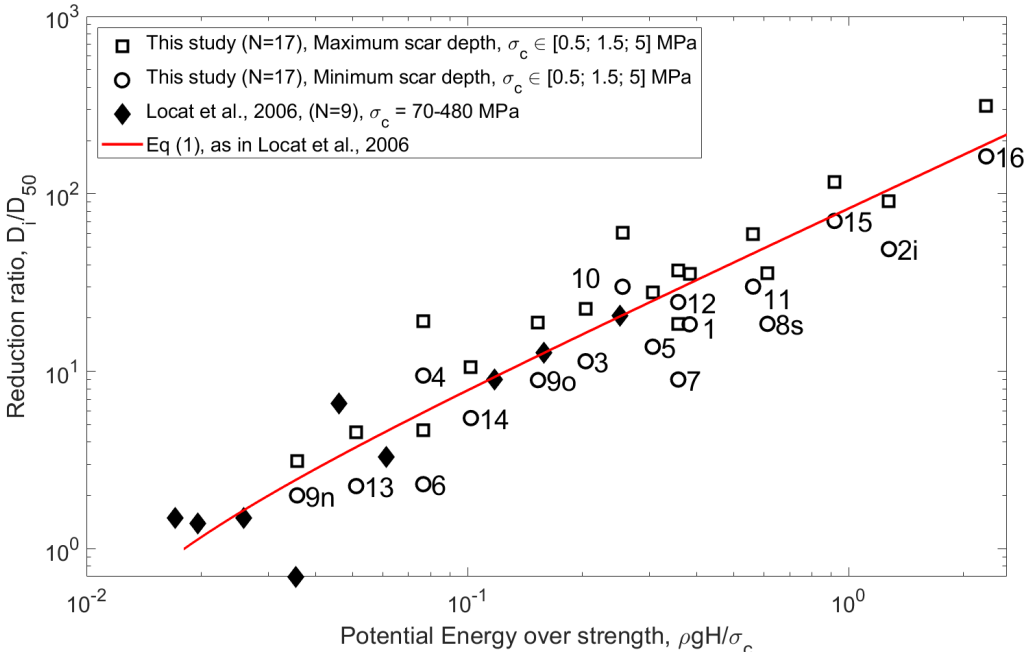

Figure S9. Same as Figure 5 but using bedrock and regolith scaling to estimate all landslide scar thickness.

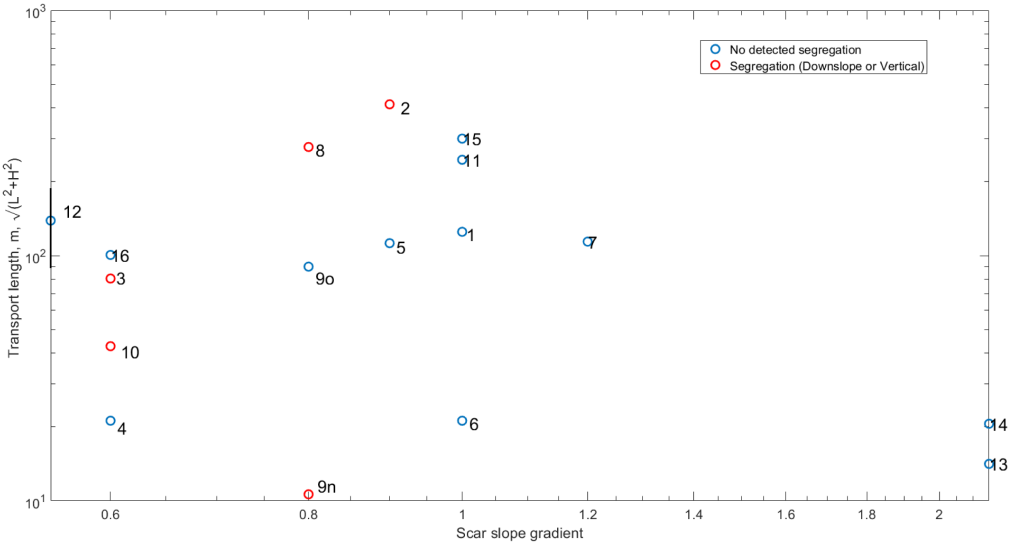

Figure S10. Transport distance vs scar gradient for the surveyed landslides. Although uncertainties on scar gradient are high, segregation seems rare for steep scar, and short transport.